Focal spot size of intense heavy ion beam — post mortem analysis of irradiated metallic foils

Maria Zhukova
Tomsk Polytechnic University, Russia, zhukova_mariya@mail.ru

A set of thin metallic foils irradiated by intense, strongly focused ^{124}Xe beam has been surveyed. High level of energy deposition by the beam in the foil near the focal plane lead to melting of the refractory material and formation of a macroscopic hole around the beam axis. The transverse beam and hole dimensions have been related by a simple analytic model. The results of the post mortem analysis of tantal and copper foils are presented and discussed.

1 Introduction

At the HHT area of GSI intense beams of energetic heavy ions are used to generate high-energy-density (HED) states in matter by their impact on solid targets [1]. In most of these experiments, an intense heavy ion beam is focused on the target to a millimeter or sub-millimeter spot. The main difficulty for measurement of the intensity distribution in the focal plane (i.e., at the target position) is a high level of energy deposition by the beam in matter which does not allow conventional diagnostic instruments like scintillation screens, wire scanners or profile grids to be used.

During the interaction with even slightly invasive diagnostic instruments, an intense focused beam can induce in matter HED states with internal energy up to several kJ/g and temperatures about 2000 – 10000 K. This leads not only to e.g., saturation and degradation of scintillation properties of a detector but to macroscopic modifications of the thermodynamical state and mechanical properties of the material. For example, most of the materials including refractory metals are melted or evaporated during the interaction with a single ion beam pulse [1, 2]. With the development of high intensity heavy ion accelerators such as SIS-100 at FAIR, the problem of non-intercepting transverse diagnostics of strongly focused beams becomes imperative.

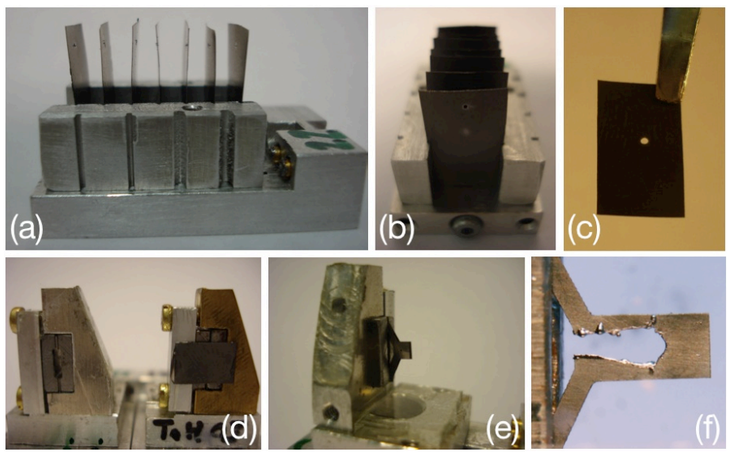

Fig. 1: *Targets used for beam diagnostics. Multi-foil "M"-target: (a) — side view, beam is coming from left; (b) — front view. "Y"-target with Ta foil: (d) — front view with and without Ta foil (c) glued on the slit diaphragm, (e) — side view on the "Y" target foil (f) behind the diaphragm.*

Contrary to non-intercepting on-line diagnostic techniques, an attempt to estimate the beam focal spot size by off-line (*post mortem*) analysis of thin tantalum and copper foils irradiated by intense ^{124}Xe beam has been made in the frame of this work. As a result of the interaction of an intense and strongly focused beam with a metallic foil, a certain area of the foil around the beam axis is heated above the melting point and a macroscopic hole is therefore formed (see Figs. 1, 3). The dimensions and shape of the hole should reveal transverse intensity distribution of the ion beam. In the following sections we describe the corresponding beam time experiments at GSI, introduce a simple model which relates beam and hole dimensions, present the obtained results and discuss limitations and further development of the method.

2 Beam time experiment

The experiment has been performed at the HHT area of GSI in July 2008. A detailed description of the experimental setup can be found in [1]. A $^{124}Xe^{48+}$ beam with initial ion energy of $E_i = 350$ AMeV delivered by SIS-18 synchrotron in $\tau \approx 800$ ns pulses and intensity of $N \sim 6 \cdot 10^9$ ions/pulse has been focused to a sub-millimeter spot inside a vacuum target chamber. The chamber is separated from the high-vacuum beam transfer channel by a 150 μm aluminum foil. The beam current profile and total number of particles were measured for every shot using fast and resonant current transformers, respectively. As a standard on-line diagnostics for beam position and size, beam-induced fluorescence of gas target (transverse emission profiles of argon ionic lines) has been employed [3], hereafter referred as *optical measurements*.

The aim of the experiment was to study thermophysical and optical properties of refractory metals (W and Ta) at melting and in hot liquid states as well as enhancement of available pyrometric temperature data with direct surface reflectivity measurements. A few targets however, have been specially designed for transverse beam diagnostics purposes (Fig. 1): two multi-foil, "M"-targets where seven thin metallic foils are installed on target tables perpendicular to the beam with 3 mm distances between the foils, and several standard "Y"-targets equipped with an additional foil glued on the diaphragm 8 mm upstream the beam focal plane. In the two M-targets, 46 μm Cu and 55 μm Ta foils, respectively have been installed. The latter Ta foils have been also used in the Y-targets.

3 Model and data processing

We presume that the dimensions of a hole are determined at the end of the beam heating pulse, the slow processes of thermal conduction are neglected. The radiative energy losses during the heating time can be neglected as well: according to the Stephan-Boltzmann law $W_{\rm rad} = A\epsilon \cdot \sigma_{\rm B} T^4$, for radiating area $A = 2\,{\rm mm}^2$, surface emissivity $\epsilon = 1$ and temperature $T = T_m^{\rm Ta} \approx 3300$ K, $W_{\rm rad} \approx 14$ W. During the heating time of $\tau \sim 1\,\mu$s, target will therefore radiate less than 10^{-4} of the total energy deposited by the beam in the foil ($\Delta E_{\rm tot} \sim 0.6$ J).

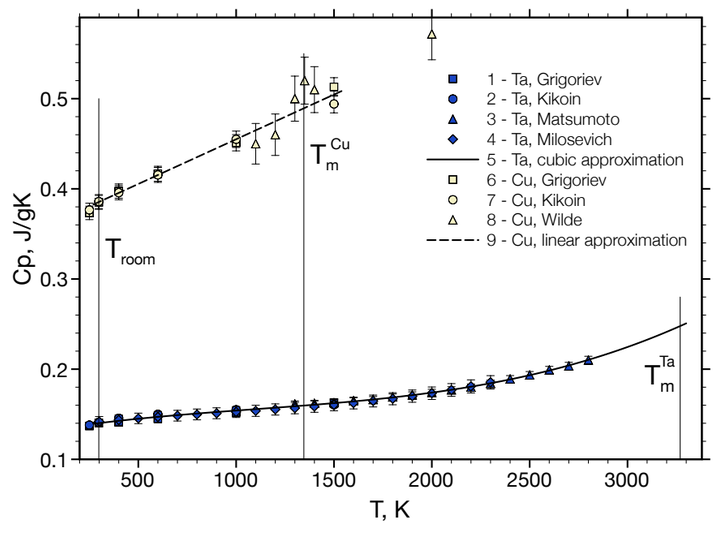

Fig. 2: *Isobaric heat capacity $C_p(T)$ and melting temperatures for tantal and copper.*

It is assumed that the necessary and sufficient condition for forming a hole is melting, i.e. the specific internal energy level in the target material

$$E_m = E_c + \Delta H, \quad E_c = \int_{T_{\rm room}}^{T_m} C_p(T)\, dT, \tag{1}$$

where E_c is the energy needed to heat the material from $T_{\rm room} = 298$ K to the melting temperature T_m, ΔH is the enthalpy of fusion and C_p is isobaric specific heat capacity. For the thin metallic foils used in the experiment, the process of heating can be treated as quasi-isobaric because the characteristic hydrodynamic relaxation time $h/C_s \ll \tau$, where h is the foil thickness, C_s is sound velocity and τ is the heating time (ion pulse duration).

Only a limited amount of experimental data on $C_p(T)$ for metals at high temperatures is available (Fig. 2). In order to calculate E_c, we have used the following polynomial r.m.s. data approximations in the interval $[T_{\rm room}, T_m]$: $C_p^{\rm Ta}(T) = 0.1308 + 3.6341 \cdot 10^{-5} T - 1.873 \cdot 10^{-8} T^2 + 5.678 \cdot 10^{-12} T^3$; $C_p^{\rm Cu}(T) = 0.3558 + 9.928 \cdot 10^{-5} T$. The relevant thermodynamic properties of Ta and Cu targets are summarized in Table **??**. The original data on $C_p(T)$ and ΔH has been taken from Refs. [4, 5, 6, 7, 8].

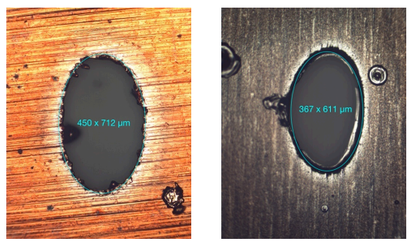

Fig. 3: *Microscope images of beam-produced holes in Cu (left) and Ta (right) foils.*

We assume the centered bivariate Gaussian distribution

$$G(x, y, \sigma_x, \sigma_y) = \frac{1}{2\pi\sigma_x\sigma_y} \exp\left[-\frac{x^2}{2\sigma_x^2} - \frac{y^2}{2\sigma_y^2}\right] \tag{2}$$

for the beam intensity and therefore the transverse specific energy deposition in the target

$$E_s = N \cdot \hat{E} \cdot G(x, y); \quad \hat{E} = \frac{1}{\rho h} \int_0^h \frac{dE}{dx}\, dx, \tag{3}$$

where N is the total number of ions in a pulse (beam intensity), $\hat{E}$ is specific energy loss by a single ion, h is thickness and ρ is density of the target. The stopping power of the target material for ^{124}Xe ions, dE/dx has been calculated using *SRIM* [9] and *ATIMA* [10] codes, taking into account the energy loss in all upstream foils, if any. Due to a considerable difference between the *SRIM* and *ATIMA* results for Cu, the *ATIMA* values for Cu and Ta were taken for further data analysis.

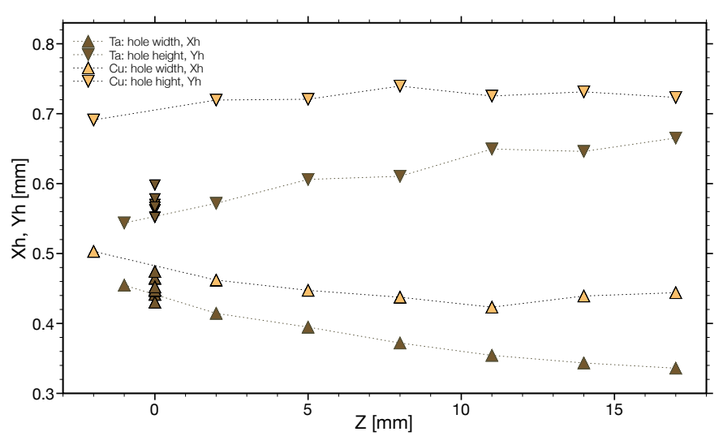

Fig. 4: *Hole dimensions in Ta and Cu foils.*

Finally, the equality $E_s = E_m$ and Eqs. (1), (2) and (3) imply the following relation between the hole $\{X_h, Y_h\}$ and the beam $\{\sigma_x, \sigma_y\}$ dimensions:

$$\begin{cases} G(\frac{1}{2}X_h, & 0, & \sigma_x, \sigma_y) & = E_m/N\hat{E} \\ G(0, & \frac{1}{2}Y_h, & \sigma_x, \sigma_y) & = E_m/N\hat{E}, \end{cases} \tag{4}$$

which can be reduced to an equation for σ_x^2

$$\exp\left[-\frac{X_h^2}{8\sigma_x^2}\right] = \frac{2\pi E_m}{N\hat{E}} K\sigma_x^2, \quad K = \frac{\sigma_y}{\sigma_x} = \frac{Y_h}{X_h}. \tag{5}$$

Given the width X_h and the heigh Y_h of an elliptic hole, the corresponding ion beam FWHM spot sizes, $\{W_x, W_y\} = 2.35 \cdot \{\sigma_x, \sigma_y\}$ can be calculated by solving Eq. (5).

After the experiment, microscope images for all target foils with the beam-produced holes were taken (Fig. 3). These images where analysed and calibrated using a multi-platform image processing code *ImageJ* [11]. For each image from both sides of a foil, the hole dimensions $\{X_h, Y_h\}$ were determined by fitting an ellipse to the visible hole boundary and the results of several such measurements were averaged. The measured hole dimensions are shown in Fig. 4 as a function of foil position along the beam axis Z. The group of points at $Z = 0$ represent the Ta "Y"-target foils.

In order to obtain the beam dimensions, the Eq. (5) has been solved numerically for every foil and every shot. For this purpose, a special batch processing *MATLAB* code has been written. The possible inaccuracy of the solutions due to a limited knowledge of melting dynamics has been accounted by assuming a large error bar corresponding to $[E_m - \frac{\Delta H}{2}, E_m + \frac{\Delta H}{2}]$ interval of specific energies required for melting.

It is interesting to note, that for any given $\{X_h, Y_h\}$ and beam energy $N\hat{E}$, Eq. (5) has two solutions, $S_1 = \{W_x^{(1)}, W_y^{(1)}\}$ and $S_2 = \{W_x^{(2)}, W_y^{(2)}\}$ or none, if the beam energy is insufficient for melting. Multiple solutions of the problem is not a unique property of the Gaussian distribution but of any beam intensity profile (e.g., Cauchy-Lorentz) which second derivative changes its sign.

4 Results and discussion

The results for the Ta "M"-target are shown in Fig. 5. The obtained FWHM beam size in horizontal (W_x, squares) and vertical (W_y, circles) directions are shown for each Ta foil as a function of its longitudinal coordinate Z. Both solutions, S_1 and S_2 are plotted. The corresponding hole dimensions are shown in the same fgr with triangles.

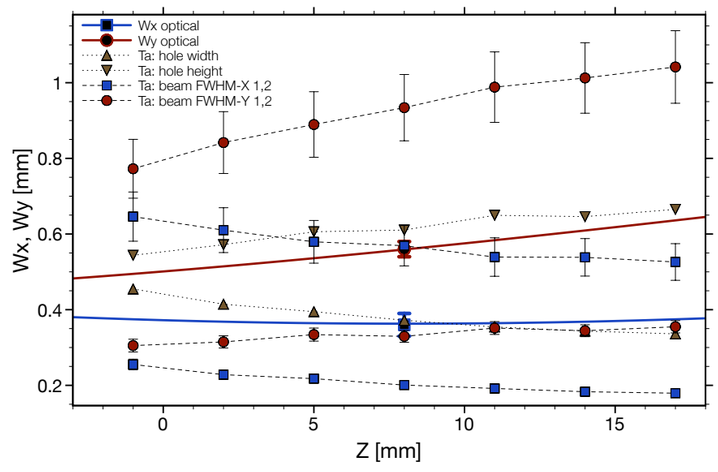

Fig. 5: *FWHM beam envelopes $\{W_x(Z), W_y(Z)\}$ for Ta "M"-target and optical measurements.*

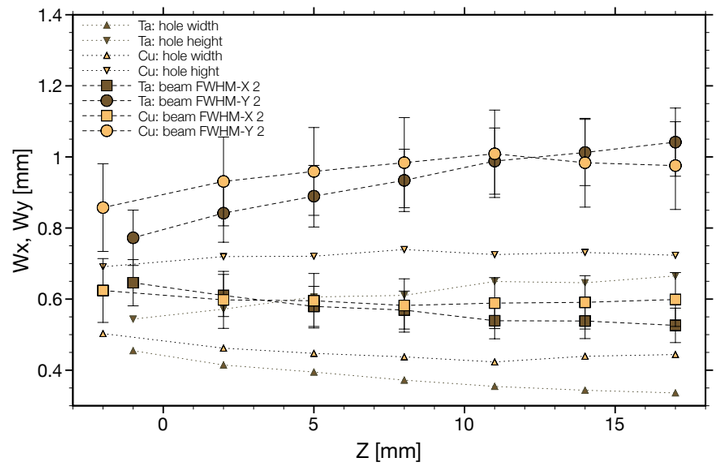

Fig. 6: *Comparison of the solutions S_2 for Ta and Cu "M"-targets.*

The results of optical beam size measurements at X-focal plane ($Z = 8$ mm) for the same beam are also shown in Fig. 5. The beam envelopes plotted by thick red and blue solid lines are results of ion-optical simulations of the quadrupole final focus system, where the transverse beam emittance values were adjusted in order to fit the results of the optical measurements. The present hole analysis gives $S_1 = \{0.20, 0.33\}$ mm, $S_2 = \{0.57, 0.93\}$ mm, whereas optical measurements suggest $S_{\rm opt} = \{0.36, 0.56\}$ mm, i.e. right in between S_1 and S_2. The aspect ratio of the beam $K \approx 1.6$ is the same for all. Despite a big difference in the values, there is no peremptory argument which would allow to immediately reject one of these three results.

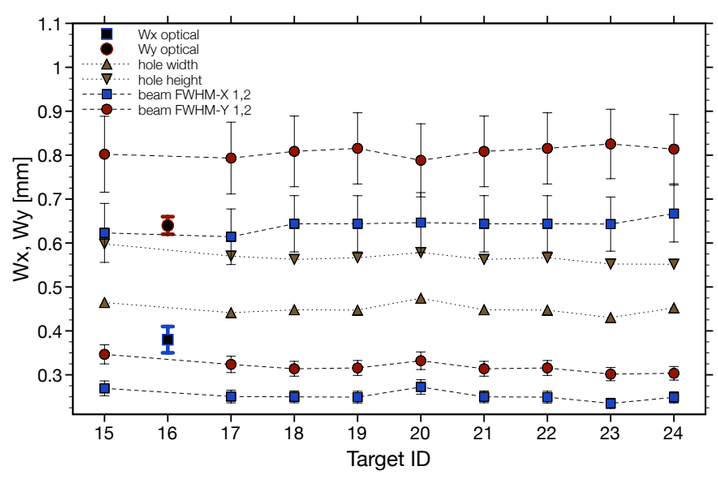

Fig. 7: *Beam dimensions calculated for "Y"-targets.*

In Fig. 6 the S_2 solutions for Ta and Cu "M"-targets are plotted together. Although the values T_m, C_p and $\{X_h, Y_h\}_i$ for Ta and Cu significantly differ, the solutions are close to each other. This indicates that the developed physical model which relates the hole and the beam dimensions is reasonable. Finally, Fig. 7 shows the results for single-foil Ta "Y"-targets. The situation here is analogous to the "M"-targets discussed above.

It is planned to extend the present work by taking into account the dynamic thermal conduction effects and studying the influence of the beam intensity distribution shape.

Acknowledgments

I wish to thank my tutor Dr. Dmitry Varentsov for his encouragement, support and advice on every aspect of the work as well as in daily live as well as Prof. D.H.H. Hoffmann, Dr. S. Udrea, and A. Hug for their friendly assistance.

References

[1] D. Varentsov et al., *Nucl. Instr. and Meth. A* **577**, 262 (2007).

[2] S. Udrea et al., *Nucl. Instr. and Meth. A* **577**, 257 (2007).

[3] D. Varentsov et al., *Contrib. Plasma Phys.* **48(8)**, 586 (2008).

[4] I.S. Grigorev and E.Z. Meilikhov (eds.), *Handbook of Physical Quantities* (Energoatomizdat, Moscow, 1991) [in Russian]; (CRC Press LLC, 1997) [in English].

[5] I.K. Kikoin (ed.) *Tables of Physical Quantities* (Atomizdat, Moscow, 1976) [in Russian].

[6] T. Matsumoto et al., in *Sensing Instrument Control Engineering (SICE-1999)*, (Ube, Yamaguchi, Japan, 1999).

[7] N.D. Milosevic et al., *Int. J. Thermophys.* **20(4)**, 1129 (1999).

[8] G. Wilde, *J. of Non-Crystalline Solids*, **307-310**, 853 (2002).

[9] `http://www.SRIM.org/`

[10] `http://www-aix.gsi.de/scheid/ATIMA1.html`

[11] `http://rsbweb.nih.gov/ij/`